CORROSION BEHAVIOR OF NI-BASE ALLOYS IN SUPERCRITICAL WATER

QIANG ZHANG, RUI TANG*, CONG LI[1], XIN LUO, CHONGSHENG LONG and KAIJU YIN
National Key Lab. For Nuclear Fuel and Materials, Nuclear Power Institute of China
P.O. Box 436, Chendu, PR China 610041
[1]China Nuclear Power Technology Research Institute
1788 West Road, Suzhou, PR China 215004
*Corresponding author. E-mail : xajttr@163.com

Received June 18, 2008
Accepted for Publication September 22, 2008

Corrosion of nickel-base alloys (Hastelloy C-276, Inconel 625, and Inconel X-750) in 500 °C, 25 MPa supercritical water (with 10 wppb oxygen) was investigated to evaluate the suitability of these alloys for use in supercritical water reactors. Oxide scales formed on the samples were characterized by gravimetry, scanning electron microscopy/energy dispersive spectroscopy, X-ray diffraction, and X-ray photoelectron spectroscopy. The results indicate that, during the 1000 h exposure, a dense spinel oxide layer, mainly consisting of a fine Cr-rich inner layer ($NiCr_2O_4$) underneath a coarse Fe-rich outer layer ($NiFe_2O_4$), developed on each alloy. Besides general corrosion, nodular corrosion occurred on alloy 625 possibly resulting from local attack of γ' clusters in the matrix. The mass gains for all alloys were small, while alloy X-750 exhibited the highest oxidation rate, probably due to the absence of Mo.

KEYWORDS : Ni-Base Alloys, Supercritical Water, Corrosion Behavior, Oxide Scale

1. INTRODUCTION

As one of the Generation IV reactor concepts, supercritical water reactors (SCWRs) are characterized by simplified design, smaller volume, and higher thermal efficiency than that of light water reactors (LWRs). Corrosion of structural materials immersed in the supercritical water (SCW) thus contained is expected to be more severe than in LWRs. Therefore, a systematic study on corrosion of candidate materials is needed before they can be safely used in nuclear reactor systems [1,2]. At present, Ferritic-martensitic (F/M) steels, austenitic stainless steels, and Ni-base alloys are considered the main candidate materials for SCWRs. A great deal of investigation on the corrosion of F/M steels and austenitic stainless steels in SCW has been reported [3-10], in contrast to the few published works on Ni-base alloys [11-15].

Our current work aims to evaluate corrosion of three Ni-base alloys (Hastelloy C-276, Inconel 625, Inconel X-750) in a SCW environment at 500 °C and 25 MPa by means of scanning electron microscopy (SEM)/energy dispersive spectroscopy (EDS), X-ray diffraction (XRD), and X-ray photoelectron spectroscopy (XPS). This represents a part of the ongoing research program on the screening of alloys for SCWR systems at the Nuclear Power Institute of China.

2. EXPERIMENTAL

Plates of Hastelloy C-276, Inconel 625, and Inconel X-750 were procured from Panzhihua Iron & Steel Co. The nominal chemical compositions of the materials are shown in Table 1, and microstructures of the as-received alloys are shown in Fig. 1. Alloy C-276 shows a homogeneous microstructure with annealing twins and its average grain size is about 40 μm (Fig. 1a). The microstructure of alloy 625 reveals an average grain size of 60 μm and clusters of bulk precipitates (about 5 μm in size) at grain boundaries (Fig. 1b). Alloy X-750 consisted of fine grains of about 20 μm average size and small precipitates (about 1 μm) both at grain boundaries and randomly distributed throughout the matrix (Fig. 1c). EDS analyses indicate γ' Ni_3(Nb,Mo) and γ' Ni_3(Al,Ti) precipitates in alloy 625 and X-750, respectively (Fig. 2).

The as-received alloys were cut into samples 40 mm × 20 mm × 1.5 mm in size and were then mechanically polished to a 1 μm diamond finish. Prior to being exposed to SCW, the samples were cleaned with acetone and ultrasonically rinsed with de-ionized water for 5 minutes.

All SCW exposure tests were performed in a 2 L autoclave at 500 °C under a pressure of 25 MPa. For the inlet water, the dissolved oxygen concentration was kept below 10 ppb by bubbling pure nitrogen through it, while

Table 1. Chemical Compositions of the Tested Materials

	C	Si	Mn	Cr	Al	Ti	Nb	Fe	Ni	Cu	Mo	Co	W	V
X-750	0.035	0.32	0.34	16.05	0.95	2.59	0.95	5.27	bal.					
625	0.045	0.39	0.29	22.04	0.13	0.15	3.96	3.38	bal.	0.004	8.19	0.03		
C-276	0.001	0.03	0.52	15.88				5.35	bal.		15.64	1.51	3.38	0.02

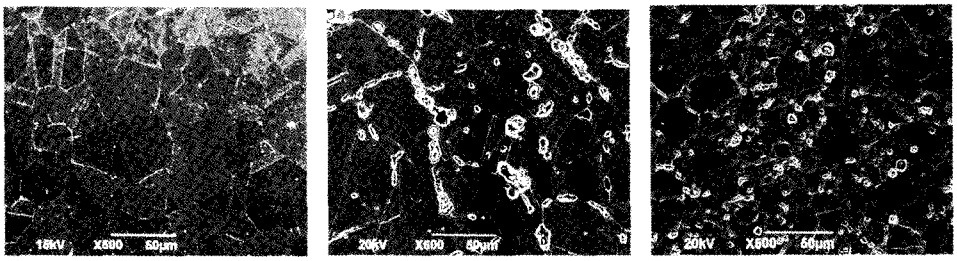

(a) (b) (c)

Fig. 1. Microstructures of the as-Received Alloys (a) C-750, (b) 625, and (c) X-750

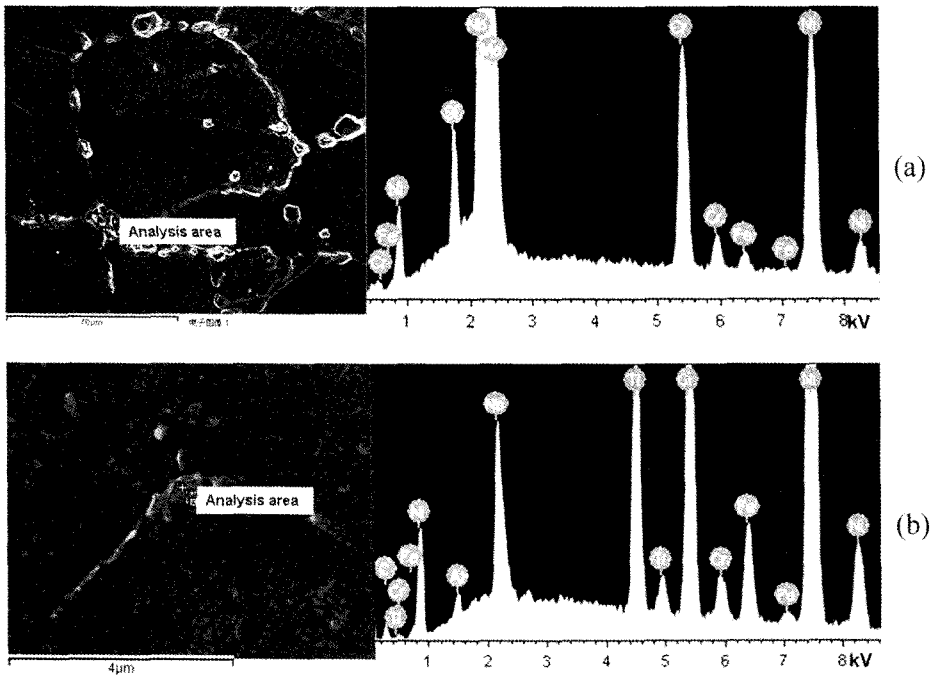

Fig. 2. EDS Analyses of the Precipitates in Alloys (a) 625 and (b) X-750

the water conductivity (at 25 °C) was kept below 0.1 μS/cm. The test conditions are shown in Table 2.

After exposure, the resulting oxide scales were characterized by mass change measurements as well as surface and cross-sectional analyses. An ESJ180-4 electric balance of accuracy 0.1 mg was used to measure the mass change of each alloy. Scanning electron microscopes (JEOL JSM-6490 and FEI Nano400) equipped with EDS were used to observe oxide morphology and thickness and to analyze the chemical compositions. Surface oxide phases were identified through X-ray diffraction (Philips X' Pert PRO MRD) using a Cu K_α radiation source. The elemental binding states and composition profiles of the oxide surfaces were characterized through X-ray photoelectron spectroscopy (XPS, Physical Electronics ESCALAB 250 system).

Table 2. Test conditions for the SCW Exposure

Parameters	Conditions
Temperature (°C)	500±5
Pressure (MPa)	25±0.5
Dissolved Oxygen (ppb)	<10 (deaerated)
Water conductivity (μS/cm)	0.1
pH	Neutrality (RT)
Test time (hours)	1000
Sampling period (hours)	100, 200, 400, 600, 800, 1000

3. RESULTS AND DISCUSSION

3.1 Plan-View Images

Alloy surface morphologies were measured for different exposure times (Fig. 3). Growth process of the oxide layers during exposure can be deduced as follows. Oxide nucleation occurs on selected sites. Fine oxide grains then grow uniformly until they connect with each other resulting in a compact layer composed of uniform grains 200 nm in size. After this, partial grains grow continuously to a size of 1 μm. The number density of the larger grains increases with time leading to oxide layer growth. The oxide layer on alloy X-750 grows faster than that on both alloys C-276 and 625 (Fig. 3).

Cracks formed on alloy C-276 after 1000 h exposure (Fig. 4a), indicating a tendency for oxide spallation. Many cauliflower-like oxides scattered on the uniform scale of alloy X-750 need further characterization (Fig. 3c). Aside from general corrosion, nodular corrosion also occurred on alloy 625 during exposure (Fig. 5). EDS mapping of the local corrosion zone indicates that Ti and Nb content are enriched, while Ni and Cr content are depleted. This indicates that the nodules originated from local attack at the precipitate clusters (γ") (Fig. 2a). When the nodule grows to a critical size (about 8 μm in diameter), the oxide spalls due to growth stresses. A hole then appears on the base layer (Fig. 4b).

3.2 Cross-Sectional Analyses

Cross-sectional morphologies of the alloys exposed for 1000 hours was also investigated (Fig. 6). After SCW exposure, the samples developed a duplex oxide structure

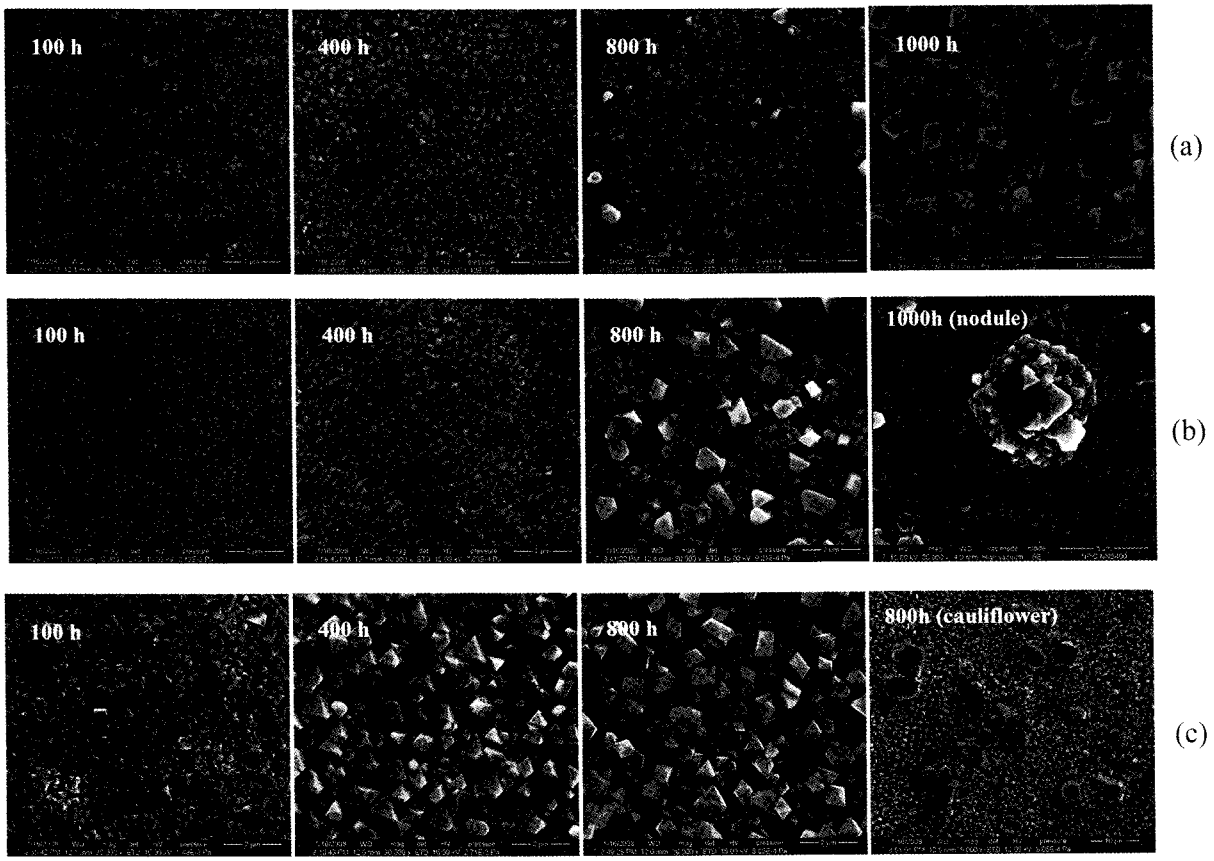

Fig. 3. Surface Morphologies for Alloys (a) C-750, (b) 625, and (c) X-750 Exposed for Different Times

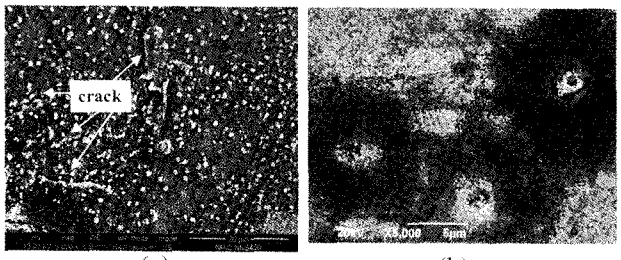

(a) (b)

Fig. 4. (a) Cracks on Alloy C-276 after 1000 Hours Exposure and (b) Holes on Alloy 625 after 800 Hours Exposure

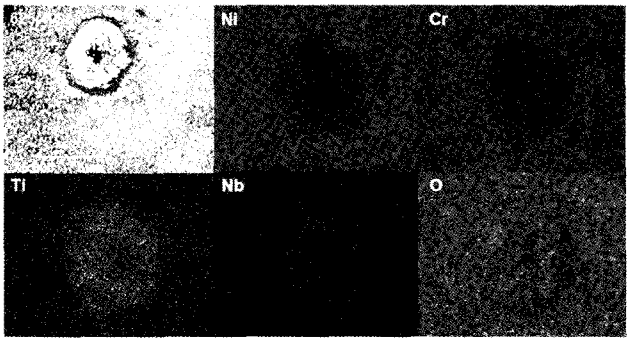

Fig. 5. EDS Mapping of the Nodule on Alloy 625 During Exposure

in which the scales consisted of coarse outer and fine inner layers. The scales on alloy C-276 and 625 (≈1 μm) exhibit good adhesion to the matrix. Alloy X-750 exhibited the thickest scale (1.5-2.5 μm) among the tested alloys, which indicates its relatively high oxidation rate.

Mo enrichment was found in the inner oxides of alloy C-276 and 625 through EDS analyses. Moreover, the

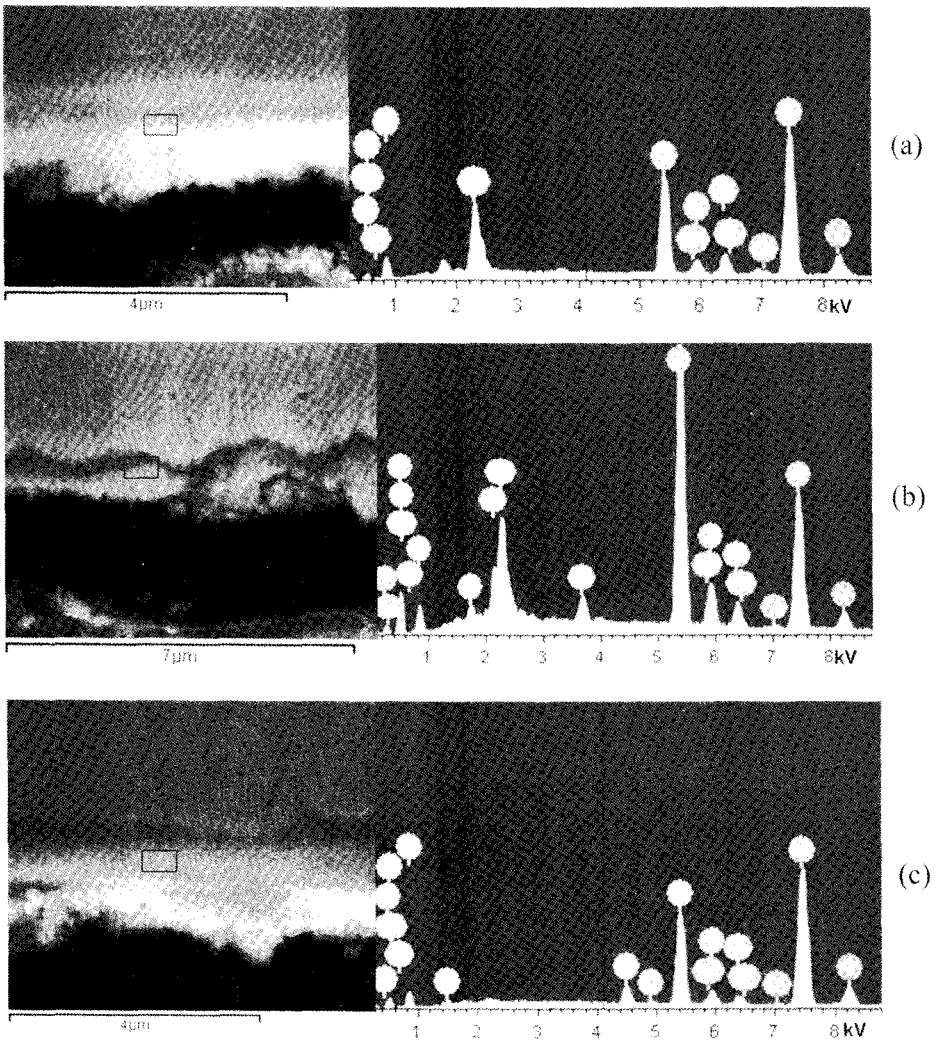

Fig. 6. Cross-Sectional Morphologies of Alloys (a) C-750, (b) 625, and (c) X-750 Exposed for 800 Hours

scale on alloy X-750 was enriched with Ti and Mn. No gradient in Cr and Fe concentrations across the oxide films was confirmed by EDS point analysis. However, further examinations, such as grazing incidence X-ray diffraction (GIXRD) and XPS in-depth profiling, will be conducted to characterize both the Cr-rich inner and Cr-poor outer spinels.

3.3 XRD and XPS Analyses

To identify the oxide phase structure, XRD analyses of the alloys exposed for 1000 hours were performed, and comparisons with the unexposed alloys were made (Fig. 7). All measured peaks in the exposed alloys are accounted for by the presence of two crystalline solids: an oxide spinel (AB_2O_4) and a metallic nickel phase representative of unoxidized base metal. Positions and relative intensities of the spinel plane reflections indicate the presence of $NiFe_2O_4$ (inverse spinel) and $NiCr_2O_4$ (normal spinel).

Further investigations of the composition of the scale

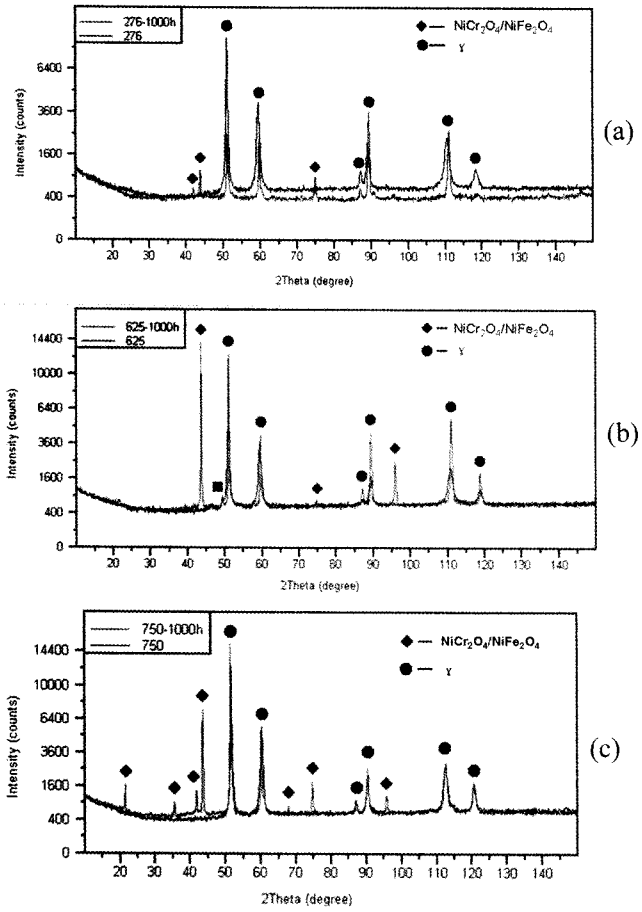

Fig. 7. XRD Patterns of the Unexposed and 1000 Hours Exposed Alloys (a) C-750, (b) 625, and (c) X-750 Exposed for 1000 Hours

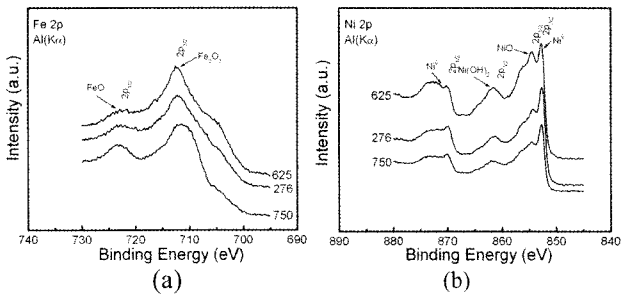

Fig. 8. XPS Spectra of the Alloys Exposed for 1000 Hours

surfaces were performed by XPS (Fig. 8). All recorded XPS peaks were decomposed. Let us consider alloy C-276 as an example. For iron, two components (peaks) were identified, namely FeO at 709.8 eV and Fe_2O_3 at 710.4 eV. Two components were also identified for O1s, namely O^{2-} at 530.1 eV and OH- at 531.8 eV. Mo3d presented two peaks: 229.5 eV (MoO_2) and 233.2 eV (MoO_3). Ni2p showed three different peaks: Ni^0 at 852.6 eV, NiO at 853.9 eV, and $Ni(OH)_2$ at 855.6 eV. All these (binding energies) are in agreement with previous findings [16]. Interestingly, no peak related to Cr was found after 15 minute argon ions sputtering. This indicates the outer oxide layer to be Ni/Fe-rich and Cr-free, which suggests the outer and inner layers to be $NiFe_2O_4$ and $NiCr_2O_4$, respectively. The spinel binary $NiFe_2O_4$-$NiCr_2O_4$ was also found on Ni-base alloys exposed to hydrogenated water at 260 °C [12,13].

3.4 Mass Gain

Mass gain as a function of exposure time was investigated for the Ni-base alloys (Fig. 9). All three alloys show good corrosion resistance in our current experiment,

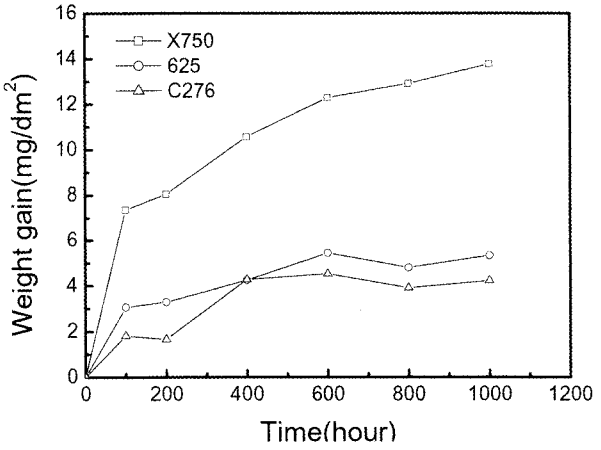

Fig. 9. Mass Gains as a Function of Exposure Time in 500 °C SCW

while X-750 exhibits a mass gain two times larger than alloys C-276 and 625, which may result from the absence of Mo. The beneficial effect of molybdenum, in terms of corrosion resistance, has already been demonstrated by many authors [17,18], where the presence of molybdenum in the passive layer was demonstrated to play a fundamental role. In general, mass gain increased with exposure time; however, an abrupt decrease occurred for alloys C-276 and 625, which may result from oxide spallation or nodular corrosion as previously discussed.

4. CONCLUSION

Dense oxide layers were observed to develop on three Ni-base alloys (Hastelloy C-276, Inconel 625, Inconel X-750) exposed to 500 °C supercritical water with 10 wppb dissolved oxygen for various exposure times up to 1000 hours. Aside from general corrosion, nodular corrosion occurs on alloy 625 due to local attack of γ" $Ni_3(Nb,Mo)$ precipitate clusters at the grain boundaries. Scales on the exposed samples are spinel oxides consisting of a fine Cr-rich inner layer (mainly $NiCr_2O_4$) underneath a coarse Fe-rich (mainly $NiFe_2O_4$) outer layer. Mass gains for all three alloys are small, and alloy X-750 showed the highest oxidation rate, which may be ascribed to the absence of Mo.

ACKNOWLEDGEMENT

The financial support by the National Basic Research Program of China (2007CB209800) is gratefully acknowledged.

REFERENCES

[1] T.C. Totemeier, D.E. Clark. Effect of transient thermal cycles in a supercritical water-cooled reactor on the microstructure and properties of ferritic-martensitic steels. Journal of Nuclear Materials, 2006, 355: 104.

[2] D.R. Novog, J. Luxat, L.K.H. Leung. Estimation of conceptual supercritical water reactor response to a small loss of coolant accident. 3rd Int. symposium on SCWR-Design and Technology, 2007: 108-117.

[3] Y. Chen, K. Sridharan, T. Allen. Corrosion behavior of ferritic-martensitic steel T91 in supercritical water. Corrosion Science, 2006, 48 (9): 2843-2854.

[4] L. Tan, Y. Yang, T. R. Allen. Oxidation behavior of iron-based alloy HCM12A exposed in supercritical water. Corrosion Science, 2006, 48 (10): 3123-2138.

[5] Yongsun Yi, Byeonghak Lee, Sungho Kim, et al. Corrosion and corrosion fatigue behaviors of 9cr steel in a supercritical water condition. Materials Science and Engineering A, 2006, 429: 161–168.

[6] X. Gao, X. Wu, Z. Zhang, et al. Characterization of oxide films grown on 316L stainless steel exposed to H2O2-containing supercritical water. Journal of Supercritical Fluids, 2007, 42: 157-163.

[7] X. Luo, R. Tang, C.S. Long, et al. Corrosion behavior of austenitic and ferritic steels in supercritical water. Nucl. Eng. Technol., 2008, 40 (2):147-154.

[8] X. Ren, K. Sridharan, T.R. Allen. Corrosion of ferritic-martensitic steel HT9 in supercritical water. Journal of Nuclear Materials, 2006, 358: 227-234.

[9] L. Tan, M.T. Machut, K. Sridharan, et al. Corrosion behavior of a ferritic/ martensitic steel HCM12A exposed to harsh environments. Journal of Nuclear Materials, 2007, 371: 161-170.

[10] Pantip Ampornrat, Gary S. Was Oxidation of ferritic-martensitic alloys T91, HCM12A and HT-9 in supercritical water. Journal of Nuclear Materials, 2007, 371: 1-17.

[11] B.P. Somerday, K.T. Wiggans, R.W. Bradshaw. Environment-assisted failure of alloy C-276 burst disks in a batch supercritical water oxidation reactor. Engineering Failure Analysis, 2006, 13: 80-95

[12] S.E. Ziemniak, M. Hanson. Corrosion behavior of NiCrMo Alloy 625 in high temperature, hydrogenated water. Corrosion Science, 2003, 45: 1595-1618.

[13] S.E. Ziemniak, M. Hanson. Corrosion behavior of NiCrFe Alloy 600 in high temperature, hydrogenated water. Corrosion Science, 2006, 48: 498-521.

[14] L. Tan, K. Sridharan, T. R. Allen. The effect of grain boundary engineering on the oxidation behavior of INCOLOY alloy 800H in supercritical water. Journal of Nuclear Materials, 2006, 348: 263-271.

[15] G.S. Was, P. Ampornrat, G. Gupta, et al. Corrosion and stress corrosion cracking in supercritical water. Journal of Nuclear Materials, 2007, 371: 176-201.

[16] D. Rats, L. Vandenbulcke, R. Herbin, R. Benoit, R. Erre, V. Serin, J. Sevely, Thin Solid Films 270 (1995) 177.

[17] G. Latha, N. Rajendran, S. Rajeswari, J. Mater. Eng. Perform. 6 (1997) 743.

[18] H.C. Brookes, J.W. Bayles, F.J. Graham, J. Appl. Electrochem. 20 (1990) 223.